Research Article Vol. 32, No. 3 / 29 Jan 2024 / Optics Express 4317
Optics EXPRESS

# Temperature-controlled spectral tuning of a single wavelength polymer-based solid-state random laser

BHUPESH KUMAR,[1,2] SEBASTIAN A. SCHULZ,[2] AND PATRICK SEBBAH[1,*]

[1]Department of Physics, The Jack and Pearl Resnick Institute for Advanced Technology, Bar-Ilan University, Ramat-Gan, 5290002, Israel
[2]SUPA, School of Physics and Astronomy, University of St. Andrews, Fife, KY16 9SS, UK
*patrick.sebbah@biu.ac.il

**Abstract:** We demonstrate temperature-controlled spectral tunability of a partially-pumped single-wavelength random laser in a solid-state random laser based on DCM [4-dicyanomethylene-2-methyl-6-(p-dimethylaminostyryl)-4H-pyran] doped PMMA (polymethyl methacrylate) dye. By carefully shaping the spatial profile of the pump, we first achieve a low-threshold, single-mode random lasing with an excellent side lobe rejection. Notably, we show how temperature-induced changes in the refractive index of the PMMA-DCM layer result in a blue shift of this single lasing mode. We demonstrate spectral tunability over an 8nm-wide bandwidth.



## 1. Introduction

Random lasers are unconventional optical cavity-based laser sources in which feedback is provided by randomly-distributed scattering particles. In the past two decades, random lasers have been the subject of intense theoretical and experimental study [1–10]. Tunability and directionality are important features that determine the application scope of any laser device in fields such as integrated spectroscopy, remote sensing, biological application [11,12] and optical communication [13]. Single wavelength random laser tunability is challenging due to the random and multimode nature of the emission spectrum, fluctuations in the emission spectrum, and lack of precise, non-invasive and reversible tuning mechanism. Spectral tunability in random lasers has been demonstrated via multiple mechanisms, including optical fiber-based random lasers [14], pump size control or scatterer concentration variation [15], gain medium thickness variation [16], dye molecule selection [17,18], or mechanical stretching [19,20]. Other tuning mechanisms include engineering absorption of light emission [21], switching modes associated with different lengths of silver nanorods in plasmonic random lasers [22], as well as electric-field-induced tunability [23]. However, all these mechanisms have been limited to the spectral tuning of broad linewidth or multimode random lasers. Tunable single-mode random laser has been reported in rare-earth-doped fiber random laser, emitting exclusively in the mid-near-infrared [25–28]. Single-mode random lasing temperature-based tunability in the visible has been demonstrated in liquid crystal-embedded random lasers, but tunability was found to be limited to a few nanometers by the nematic-isotropic transition temperature [24]. To the best of our knowledge, single mode tunable random laser in the visible has not yet been reported.

Recently, we have demonstrated that using an iterative pump shaping optimization method, selective excitation of a particular mode of the multimode emission spectrum and single-mode operation with high side-lobe rejection can be achieved [29–31]. However, it is not possible to achieve lasing at any arbitrary desired wavelength, but only at wavelengths corresponding to

#505162 https://doi.org/10.1364/OE.505162
Journal © 2024 Received 6 Sep 2023; revised 21 Nov 2023; accepted 23 Nov 2023; published 25 Jan 2024

Optics EXPRESS

lasing modes of the discrete multimode emission spectrum. Overcoming this limitation would add tunability to this technique and offer full spectral control of the random laser. In this paper, we report single-wavelength spectral tuning in a dye-doped solid-state random laser. Random lasers (RLs) typically produce multimode coherent light due to the random distribution of scattering particles. By combining the technique of spatial pump shaping together with the negative thermal coefficient of the refractive index of PMMA polymer, we are able to achieve single wavelength spectral control of a random laser on a single device. Specifically, we show piecewise spectral tunability over a bandwidth of 8 nm.

## 2. Sample fabrication

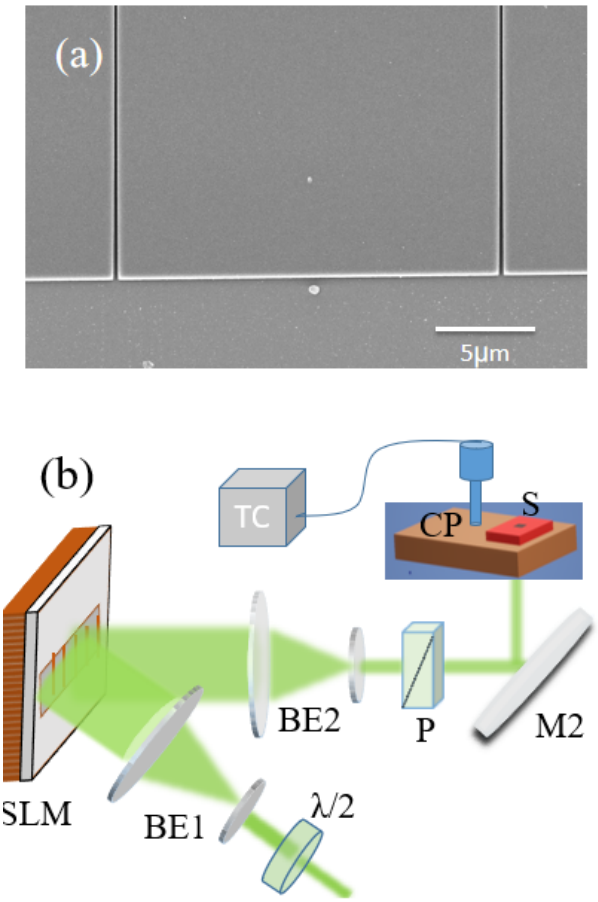


**Fig. 1.** (a) High resolution SEM image of the small section of the sample from the top showing air grooves carved into the PMMA-DCM layer. (b) Schematic of the experimental setup. BE1 and BE2: Beam expanders; P: Polarizer, SLM: Spatial light modulator; M2: Mirror; S: Sample; TC: Temperature controller; CP: Copper plate;

Disorder structures are made up of a polymer-doped layer, which is spin-coated on a transparent fused silica wafer. The passive polymer host is poly(methyl methacrylate) (PMMA) having a molecular weight of 49500, and is doped at a concentration of 5 % weight with the commercial laser dye DCM. The active layer of 600 nm was obtained by spin-coating a doped-polymer solution at 1000 rpm for 60 seconds on a fused silica wafer (Edmund optics) and post-baking it

Optics EXPRESS

at 120°C for 2 hours in an oven [31]. The fluorescence spectrum of the dye is centered around 600 nm; it has a good fluorescence quantum yield of 0.66 [32] and a large stoke shift (100 nm), which means it does not reabsorb the emitted light. The silica wafer has a refractive index of 1.45, compared to 1.54 for the PMMA-DCM layer. To fabricate one dimensional(1D)-disorder samples, 125 randomly distributed parallel grooves, each 200 nm wide and 50 μm long, covering a total length of 1000 $\mu$m, were carved into the PMMA-DCM layer using e-beam lithography (CRESTEC/CABL-9000C) (see Fig. 1(a)). After exposure samples are developed in a 1:3 solution of MIBK: IPA for 20 sec, resulting in dielectric sections with an average length of 8 μm separated by air gaps of 200 nm. The fabrication method ensures a high refractive index contrast of 0.54 between air grooves and the polymer layer, which helps in achieving random lasing action at a low threshold.

## 3. Experimental setup

A schematic of the experimental setup is shown in Fig. 1(b). The setup consists of a frequency-doubled mode-locked Nd:YAG laser (EXPLA PL2230: 532 nm, 20 ps, maximum output energy 28 mJ, repetition rate 1-50 Hz). The incoming laser beam is first expanded 5X using a beam expander (BE1) and spatially modulated by a reflective spatial light modulator (SLM) (Holoeye HES 6001, 1952 x 1088 pixels, pixel size 8.0 μm). The SLM is placed in the object plane of a beam expander (BE2) used in reverse mode with 4X reduction and is imaged on the sample from the bottom using mirror M2. A grayscale image is generated by a MATLAB code projected on SLM to create a laser strip whose width and length can be adjusted according to the sample dimensions. The disordered structure is precisely aligned with the laser strip under a fixed-stage Zeiss microscope (AxioExaminer A1) and imaged using an Andor Zyla sCMOS camera (22 mm diagonal view, 6.5 μm pixel size) using a 10X objective. The laser emission is collected along the length of the sample in x-y plane through a multimode optical fiber connected to a Horiba iHR550 imaging spectrometer equipped with a 2400 $mm^{-1}$ and 1200 $mm^{-1}$ grating and Synapse CCD detection system (sampling rate 1 MHz, 1024 x 256 pixels, 26 μm pixel pitch). The entrance slit is 50 μm, resulting in a spectral resolution of 20 pm.

## 4. Results

When the sample undergoes optical pumping, amplified spontaneous emission experiences multiple scattering. This provides in turn coherent optical feedback, enabling random lasing oscillations with sharp emission linewidth. Above the threshold, multimode lasing is achieved (illustrated in Fig. 2(a)). The resulting spectrum displays randomly positioned, distinct lasing peaks, each exhibiting a typical linewidth of 0.2 nm, constrained by the resolution of the spectrometer. We also demonstrate spectral reproducibility by manufacturing three samples with identical disorder configurations on the same substrate. We fabricate 3 samples each of length 1000 $\mu$m, width 50 $\mu$m having 125 air grooves with an identical deviation of 3 $\mu$m for each sample from the mean spatial period of 8 $\mu$m. These samples are then subjected to uniform pumping at the same pump power, and their respective emission spectra are recorded. Remarkably, all three samples yield identical emission spectra, as depicted in Fig. 2(b). The high degree of spectral reproducibility is attributed to the highly precise e-beam nanolithography fabrication technique. Once the pump intensity reaches above the lasing threshold, the output intensity increases manifold. This nonlinear increase in output intensity confirms the onset of random lasing action. By linear fit, the lasing threshold value is found to be 35 nJ for a pump size of 450 $\mu$m X 50 $\mu$m (Fig. 3(a)). The directivity of our random laser is assessed, with half of the emission intensity confined within ± 2.5 degrees from the center of the sample. This is found by scanning a 20X microscope objective placed at a distance of 10 cm from the sample edge to collect emission in a direction orthogonal to the sample length. Directional measurements are shown in inset Fig. 3(a).

Optics EXPRESS

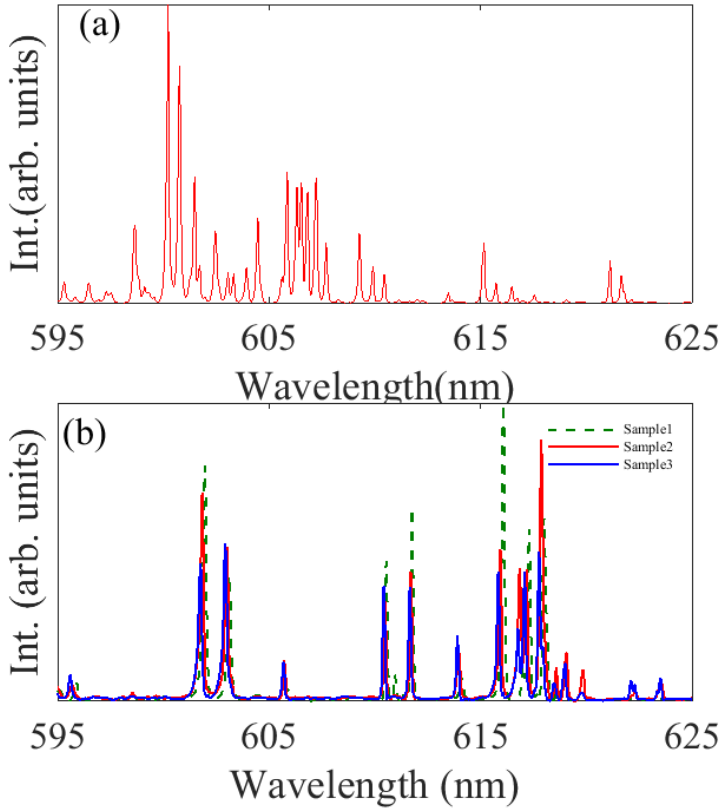


**Fig. 2.** (a) Multimode Random laser emission spectra obtained after pumping the sample uniformly above the threshold, sample length 1000 $\mu$m, pump size 1000 $\mu$m X 50 $\mu$m. (b) Almost identical emission spectra were recorded for 3 different samples each length = 1000 $\mu$m, width 50 $\mu$m having 125 grooves with identical disorder configurations. The emission spectrum recorded is recorded at a constant pump power with pump dimensions 1000 $\mu$m X 50 $\mu$m.

We also examined the photostability of our quasi-1D random laser by subjecting the sample to uniform pumping using the same experimental conditions as described earlier. The pump energy was held constant at 50 nJ, employing a pump size of 450 μm x 50 μm, and a pump laser repetition rate of 10 Hz. In Fig. 3(b), we present the integrated emission intensity graphed against the laser pulse number. The photostability of the laser was observed to be 28380 pulses, equivalent to approximately 47.3 minutes, during which the integrated laser emission intensity reduced to half of its original integrated lasing intensity. The observed decay of laser emission is due to the photobleaching of the dye under continuous laser pulses exposure. It does not have any impact on the nature of RL emission, except on its intensity. The exponential decay we found describes well the lifetime decay of the dye.

We would also like to mention that our laser samples has been continuously (10Hz repetition rate) pumped high above threshold (50nJ) for hours. The lifetime (defined here as the time when emission intensity is reduced by half) was found to be about 50 min. We also found (not reported) that just above threshold, the dye is photostable, with negligible photodegradation [33]. Photobleaching of exposed standard organic dyes occurs in minutes or even in seconds (which necessitates to use a jet in dye lasers). Here the polymer matrix naturally protects the dye molecules from oxidation and even provides with a regenerative mechanism, which results

Optics EXPRESS

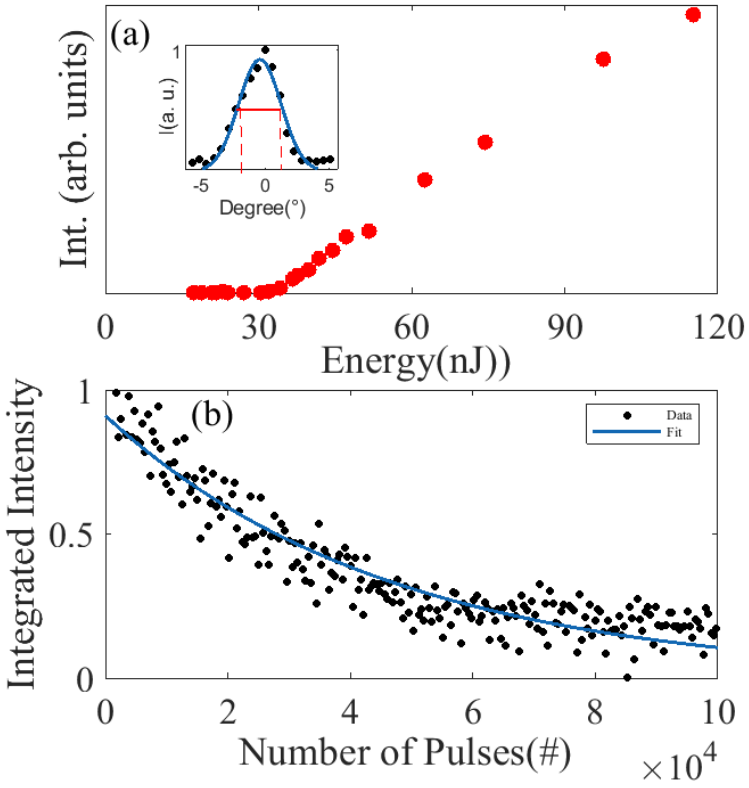


**Fig. 3.** (a) The integrated intensity of the emission spectrum with increasing pump energy (nJ). inset: Angular distribution of the integrated output intensity of random laser emission at a distance of 10 cm from the sample edge, the blue line is a Gaussian fit. (b) Integrated intensity as a function of the number of pump pulses for the random laser. The pump energy is about 50 nJ for a uniform pump of size 450 $\mu$m X 50 $\mu$m at a repetition rate of 10 Hz. The blue line is an exponential fit.

in a much longer photostability, enough for us to carry out several optimizations. Polymer encapsulation has a protective as well as regenerative role that has been reported in the literature [34].

To achieve singlemode lasing at any of the lasing wavelengths of the multimode emission spectrum(Fig. 4(b)), we apply a nonuniform intensity profile to the pump beam by modulating the SLM. We implement an iterative optimization method [29,31] to find the optimal pump profile for which modes other then the target mode are suppressed. Here we use Nelder-Mead simplex algorithm implemented in the fminsearch function of MATLAB to optimize the pump profile. We slightly modified the fminsearch function by setting the initial step (usually the $\delta$ parameter in fminsearch) to 1.0 in order to explore a larger region of the 32-dimensional space. The number of pixels (32) was chosen as a compromise between sensitivity and computation time. The Matlab-generated image that is sent to the SLM is made up of 32 intensity blocks, each of which is encoded on 256 levels of grey and projected onto the sample. To start the optimization process, we choose 32 column-vectors $V_i$ from the 32 x 32 binary Hadamard matrix as the initial vertices.

The pump profile P(x) is therefore written as $P(x) = \frac{1}{255}\sum_{i=1}^{32}\beta_i V_i$ where $\beta_i$ takes discrete values in the range [0,255]. Each vector $\beta_i$ corresponds to a particular pump profile associated with a particular emission spectrum $I(\lambda)$. The optimization algorithm uses the inverse of the extinction ratio, $\eta = I_t/I_o$, as its cost function and aims for its minimization, where $I_t$ is the peak

Optics EXPRESS

intensity of the targeted mode and $I_o$ is the highest intensity among all other modes except the targeted mode. To find the optimized pump profile, the algorithm iteratively generates a new pump profile, applies it to the pump stripe, acquires the emission spectrum averaged over 10 shots, and computes the cost function. Mode selection and single mode operation at the lasing wavelength of $\lambda$ = 602.60 nm are achieved after the convergence of the iterative optimization, as shown in Fig. 4(c). After 250 iterations, the algorithm converges to a pump profile that suppresses modes other than the targeted mode. The selected lasing mode has a sidelobe rejection ratio (measured as the ratio of the peak intensity count of the target mode w.r.t. maximum noise level in the spectrum) of 800, which corresponds to 29 dB. The next highest intensity count, except for the target mode, in the emission spectrum is 4 counts, which is close to the average noise level present in the spectrum. We also tested the robustness of our pump profile optimization method to achieve single mode lasing by selecting 50 different lasing modes on different samples. Figure 4(d) shows the sidelobe rejection of selected modes. All the modes are selected with an excellent side-lobe rejection of more than 20 dB.

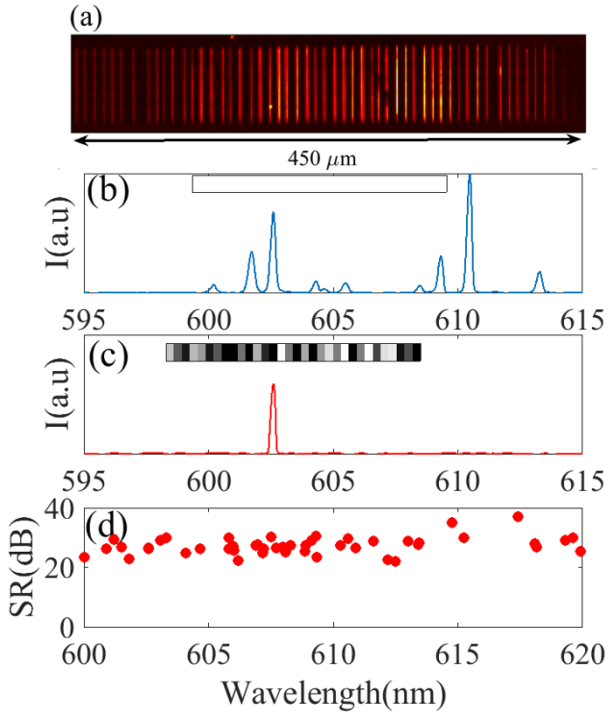


**Fig. 4.** (a) Optical microscope image of field intensity distribution near the sample surface when pumped above the threshold. (b) Multimode emission spectra for a uniform pump strip of size 450 $\mu$m X 50 $\mu$m. (c) Singlemode lasing at $\lambda$= 602.60 nm after an iterative pump optimization process. During optimization, all the spectra are recorded with a grating element of 1200 $mm^{-1}$. Inset shows the optimized pump profile in grayscale. (d) Iterative optimization of pump shaping has been applied to select 50 lasing modes. The sidelobe rejection ratio(SR) for each individually selected lasing mode w.r.t maximum noise count in the emission spectrum is plotted in log representation (dB).

Next, we demonstrate how the emission wavelength of the selected lasing mode can be tuned by changing the temperature of the sample. RL sample was positioned on a copper plate featuring a rectangular hole. Placement of the sample over the hole, enabled us to pump the RL sample from the bottom. The copper plate was connected to a heating probe to heat the sample and

Optics EXPRESS

a sensor to monitor the temperature. Figure 5(a) shows the blue shift of single-mode random laser emission initially centered at $\lambda$ = 602.60 nm, when temperature is increased. The inset in Fig. 5(a) shows the linear temperature dependence of the spectral shift. A linear fit gives a slope of d$\lambda$/dT= -0.02 nm/°C., which means that a 5 °C increase results in a spectral shift of 0.1 nm. Overall, we obtained a total shift of 1 nm between 25 °C to 75 °C. When the sample is cooled down to 25 °C, the initial spectral position is recovered and the process is perfectly reversible. This behavior is easily explained by the fact that PMMA polymer has a negative thermal coefficient of refractive index [35–37]. Its refractive index therefore decreases with increasing temperature, which results in a decrease in the optical path length within the polymer layer and a blue-shift. This process is reversible.

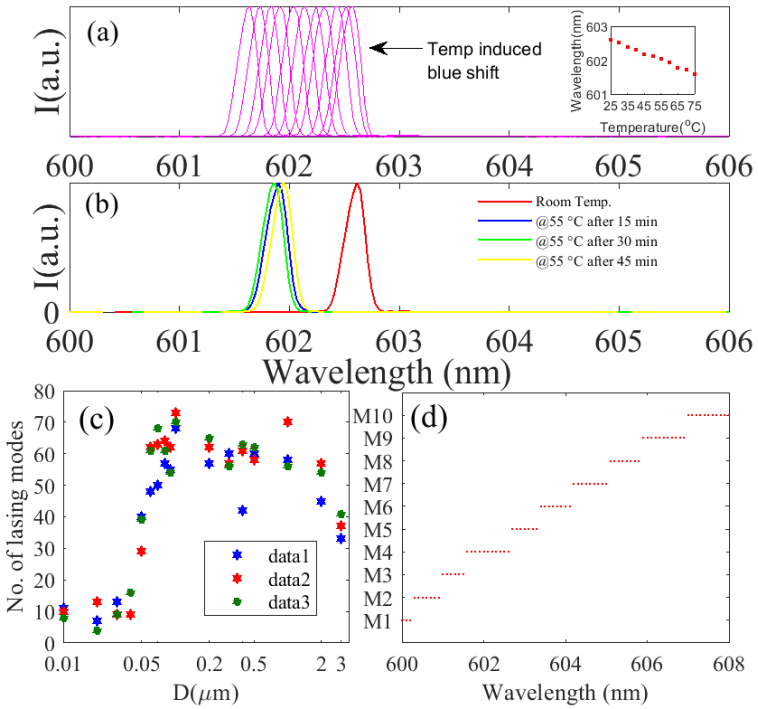


**Fig. 5.** (a) The spectral blue shift of 1 nm in the single mode lasing spectrum at $\lambda$ = 602.60 nm with increasing temperature of the polymer layer. The figure in the inset shows the temperature vs wavelength plot.(b) Emission spectrum stability at constant temperature. The emission spectrum was recorded at an interval of 15, 30, 45 minutes when the sample was heated to a constant temperature of 55°C. (c) Number of lasing modes for three different sample sets plotted as a function of increasing deviation (D) from the mean periodic position of 8 $\mu m$ in a sample of length 1000 $\mu m$ having 125 air grooves. (d) Piecewise spectral tunability over a bandwidth of 8 nm by tuning of 10 different individually selected lasing modes M1= 600.2 nm, M2= 600.9 nm, M3= 601.50 nm, M4= 602.6 nm, M5= 603.3 nm, M6= 604.1 nm, M7= 605.00 nm, M8= 605.800 nm, M9= 606.900 nm, M10= 608.00 nm.

We also performed a spectral stability test at a constant temperature higher than room temperature in a minimum airflow lab environment. An optimally-pumped lasing sample emitting light at $\lambda$= 602.60 nm is supplied with constant heat to achieve a wavelength shift of 0.60 nm at sample temperature of 55 °C. The emission spectra are recorded at 3 intervals of 15 minutes each. Lasing emission at @$\lambda$= 602.00 nm remains stable within ± 0.1 nm as shown in Fig. 5(b).

Optics EXPRESS

Since all lasing modes within the multimode spectrum can be selected individually [31], the tuning range can be in principle extended over the whole gain curve by hopping from mode to mode. To demonstrate piecewise tunability by mode hopping over a broader frequency range, we need first to identify disordered structures that provide a free spectral range smaller than the frequency shift we can achieve with a single lasing mode (typically 1 nm). Ideally, we need 10-15 modes within 8 to 10 nm spectral bandwidth of the gain curve. Interestingly, by varying the degree of disorder, the spectral density of lasing modes varies, as shown in Fig. 5(c) where the average number of lasing modes is plotted as a function of disorder deviation from the mean periodic position. Here, a 1000 $\mu$m sample with 125 air grooves has been considered, with increasing disorder ranging from 0.1 $\mu$m to 3 $\mu$m deviation from the mean spatial period of 8 $\mu$m. The reason for it is that the spatial confinement of the eigenmodes increases with increasing disorder, resulting in an increasing number of lasing modes able to reach threshold. We found that a disorder pattern with a deviation of $\pm$ 0.5 $\mu$m is enough to yield an average of 13 lasing modes within the wavelength range of 600 nm to 608 nm. We choose a pump length of 450 $\mu$m and run iterative optimization of the pump profile to select 10 lasing modes distributed over the range of 600-608 nm. The thermal-induced spectral shift is recorded for all the modes. Single-wavelength piecewise broadband tunability by mode hopping is achieved over 8 nm, as shown in Fig. 5(d).

## 5. Conclusion

In this paper, we have used a stable solid-state dye-based random laser to demonstrate temperature-induced tunability in the visible. By enforcing singlemode operation using pump shaping method, we have shown how temperature-induced change of the refractive index can achieve spectral tunability. In contrast to other mechanisms reported in the literature, our proposed method ensures singlemode tuning, it is non-invasive and does not require any modification of the sample. This random laser offers the freedom to control the free spectral range (FSR) by changing the degree of disorder. We have demonstrated that the emission wavelength of any individually selected lasing mode can be continuously blue-shifted by up to 1 nm when increasing the temperature of the PMMA-DCM layer. By hoping from one mode to another, we have demonstrated a remarkable wavelength tunability of 8 nm. This tunability range can in principle be further increased by exploring different disorder configurations and dyes. Such a tunable random laser offers the advantage of simplicity of fabrication, wide tunable bandwidth, compact in size, and the ability to operate in harsh environments compared to conventional tunable lasers that might be bulky, or require precise tuning and control mechanisms, and have limited spectral bandwidth. This single-wavelength tunable random laser holds promising potential for future applications for on-chip tunable laser sources as well as wearable temperature sensors. Because they are easy to fabricate and to integrate e.g. in optofluidics, the on-chip tunable random laser could serve to improve biomedical testing and imaging, including fluorescence, endoscopy, and confocal microscopy, by enabling precise tuning of laser wavelengths for improved targeting of biological markers and image quality. Such lasers can also be used as a versatile light source for portable spectroscopic applications, including environmental monitoring, gas detection, and material characterization, with wavelength tunability enabling adaptability to diverse target molecules and materials and multispectral imaging. Compact tunable random lasers could be integrated into next-generation display technologies. The ability to control the emission properties makes them suitable for applications in augmented reality, holography, and advanced lighting solutions, as well.

We also point out that we did not intend to demonstrate in this work the ultimate laser device. But this piece of data gives good indication that one can expect reasonable performances by e.g. improving the fabrication process, choosing a less porous polymer or a longer-lived dye (e.g the MD7 has been identified as a potential good candidate, with almost no bleaching under illumination at 355nm).

Optics EXPRESS

**Funding.** Engineering and Physical Sciences Research Council (EPSRC[EP/V029975/1]); PICS-ALAMO; Planning and Budgeting Committee of the Council for Higher Education of Israel (2015-2018); United States-Israel Binational Science Foundation (BSF #2022158, NSF/BSF #2015694, NSF/BSF #2021811); Israel Science Foundation (1871/15, 2074/15, 2630/20).

**Acknowledgement.** We extend our heartfelt appreciation to Dr. Leonid Wolfson for his unwavering dedication to the lab, and to Dr. Yossi Abulafia for his valuable assistance with the fabrication process. We are grateful to the Bar-Ilan Institute of Nanotechnology and Advanced Materials for providing us access to their fabrication facilities.

**Disclosures.** The authors declare no conflicts of interest.

**Data availability.** Data underlying the results presented in this paper are not publicly available at this time but may be obtained from the authors upon reasonable request.

## References

1. H. Cao, Y. G. Zhao, S. T. Ho, *et al.*, "Random laser action in semiconductor powder," Phys. Rev. Lett. **82**(11), 2278–2281 (1999).
2. C. Vanneste and P. Sebbah, "Selective Excitation of Localized Modes in active random media," Phys. Rev. Lett. **87**(18), 183903 (2001).
3. C. J. S. de Matos, L. S. Menezes, A. M. Brito-Silva, *et al.*, "Random Fiber Laser," Phys. Rev. Lett. **99**(15), 153903 (2007).
4. M. Gaio, D. Saxena, J. Bertolotti, *et al.*, "A nanophotonic laser on a graph," Nat. Commun. **10**(1), 226 (2019).
5. J. Liu, P. D. Garcia, S. Ek, *et al.*, "Random nanolasing in the Anderson localized regime," Nat. Nanotechnol. **9**(4), 285–289 (2014).
6. S. Schönhuber, M. Brandstetter, T. Hisch, *et al.*, "Random lasers for broadband directional emission," Optica **3**(10), 1035–1038 (2016).
7. D. N. Dirin, R. T. Lechner, G. Fritz-Popovski, *et al.*, "Random lasing with systematic threshold behavior in films of CdSe/CdS core/thick-shell colloidal quantum dots," ACS Nano **9**(10), 9792–9801 (2015).
8. H. Liang, B. Meng, G. Liang, *et al.*, "Electrically Pumped Mid-Infrared Random Lasers," Adv. Mater. **25**(47), 6859–6863 (2013).
9. B. Abaie, E. Mobini, S. Karbasi, *et al.*, "Random lasing in an Anderson localizing optical fiber," Light: Sci. Appl. **6**(8), e17041 (2017).
10. F. Lahoz, A. Acebes, T. G. Hernández, *et al.*, "Random lasing in brain tissues," Org. Electron. **75**, 105389 (2019).
11. L. Abeg ao, A. Pagani, S. Zílio, *et al.*, "Measuring milk fat content by random laser emission," Sci. Rep. **6**(1), 35119 (2016).
12. S. D. Armas-Rillo, F. F. Reading, D. L. Ravelo, *et al.*, "Random lasing as a sensing tool in brain samples of an animal model of Huntington's disease," Appl. Phys. Lett. **121**(12), 123701 (2022).
13. D. Wiersma, "The physics and applications of random lasers," Nat. Phys. **4**(5), 359–367 (2008).
14. Z. Hu, J. Xia, Y. Liang, *et al.*, "Tunable random polymer fiber laser," Opt. Express **25**(15), 18421–18430 (2017).
15. B. Kumar, R. Homri, and P. Sebbah, "2D tunable all-solid-state random laser in the visible," Sci. Rep. **13**(1), 8337 (2023).
16. J. Tong, X. Shi, S. Li, *et al.*, "Tunable plasmonic random laser based on a wedge shaped resonator," Org. Electron. **75**, 105337 (2019).
17. J. Ziegler, C. Wörister, C. Vidal, *et al.*, "Plasmonic Nanostars as Efficient Broadband Scatterers for Random Lasing," ACS Photonics **3**(6), 919–923 (2016).
18. Z. Wang, X. Meng, A. V. Kildishev, *et al.*, "Nanolasers Enabled by Metallic Nanoparticles: From Spasers to Random Lasers," Laser Photonics Rev. **11**(6), 1700212 (2017).
19. T. Zhai, J. Chen, L. Chen, *et al.*, "A plasmonic random laser tunable through stretching silver nanowires embedded in a flexible substrate," Nanoscale **7**(6), 2235–2240 (2015).
20. Y. Lee, C. Chou, Z. Yang, *et al.*, "Flexible random lasers with tunable lasing emissions," Nanoscale **10**(22), 10403–10411 (2018).
21. R. G. S. EI-Dardiry and A. Lagendijk, "Tuning random lasers by engineered absorption," Appl. Phys. Lett. **98**(16), 161106 (2011).
22. J. Zhang, F. Wang, S. Ghafoor, *et al.*, "Tunable Plasmonic Random Laser Based on Emitters Coupled to Plasmonic Resonant Nanocavities of Silver Nanorod Arrays," Adv. Opt. Mater. **10**(10), 2200426 (2022).
23. Q. Song, L. Liu, L. Xu, *et al.*, "Electrical tunable random laser emission from a liquid-crystal infiltrated disordered planar microcavity," Opt. Lett. **34**(3), 298–300 (2009).
24. Q. Song, S. Xiao, X. Zhou, *et al.*, "Liquid-crystal-based tunable high-Q directional random laser from a planar random microcavity," Opt. Lett. **32**(4), 373–375 (2007).
25. R. Ma, X. Quan, H. Wu, *et al.*, "20-watt-level single transverse mode narrow linewidth and tunable random fiber laser at 1.5 μm band," Opt. Express **30**(16), 28795–28804 (2022).
26. J. Liu, Z. Tong, W. Zhang, *et al.*, "Switchable and tunable multi-wavelength erbium-doped random distributed feedback fiber laser based on a compound filter," Optik **241**, 167015 (2021).
27. H. Wu, B. Han, and Y. Liu, "Tunable narrowband cascaded random Raman fiber laser," Opt. Express **29**(14), 21539–21550 (2021).

Optics EXPRESS


28. X. Du, H. Zhang, X. Wang, *et al.*, "Tunable random distributed feedback fiber laser operating at 1$\mu$m," Appl. Opt. **54**(4), 908–911 (2015).
29. N. Bachelard, S. Gigan, X. Noblin, *et al.*, "Adaptive pumping for spectral control of random lasers," Nat. Phys. **10**(6), 426–431 (2014).
30. N. Bachelard, J. Andreasen, S. Gigan, *et al.*, "Taming Random Lasers through Active Spatial Control of the Pump," Phys. Rev. Lett. **109**(3), 033903 (2012).
31. B. Kumar, R. Homri, S. Priyanka, *et al.*, "Localized modes revealed in random lasers," Optica **8**(8), 1033–1039 (2021).
32. A. Tagaya, T. Kobayashi, S. Nakatsuka, *et al.*, "High Gain and High-Power Organic Dye-Doped Polymer Optical Fiber Amplifiers: Absorption and Emission Cross Sections and Gain Characteristics," Jpn. J. Appl. Phys. **36**(5R), 2705 (1997).
33. V. W. Chen, N. Sobeshchuk, C. Lafargue, *et al.*, "Three-dimensional organic microlasers with low lasing thresholds fabricated by multiphoton and UV lithography," Opt. Express **22**(10), 12316–12326 (2014).
34. F. Howell Brent and G. Kuzyk Mark, "Lasing action and photodegradation of Disperse Orange 11 dye in liquid solution," Appl. Phys. Lett. **85**(11), 1901–1903 (2004).
35. X. Zhu and D. Lo, "Temperature tuning of output wavelength for solid-state dye lasers," J. Opt. A: Pure Appl. Opt. **3**(3), 225–228 (2001).
36. F. J. Duarte and R. O. James, "Tunable solid-state lasers incorporating dye-doped, polymer–nanoparticle gain media," Opt. Lett. **28**(21), 2088–2090 (2003).
37. F. J. Duarte, A. Costela, I. Garcia-Moreno, *et al.*, "Measurements of $\delta n/\delta T$ in Solid-State Dye-Laser Gain Media," Appl. Opt. **39**(34), 6522 (2000).